









Prediction of the residual stress-strain state of butt and tee joints of Al-Mg-Mn aluminium alloy produced by consumable electrode pulse-arc welding

Shiyi Gao¹, Volodymyr Korzhyk^{1,2}, Zhe Liu¹, Vladyslav Khaskin^{1,2*},
Yunqiang Zhao^{1*}, Yevhenii Illiashenko¹, Andriy Alyoshin², Viktor Kvasnytskyi³,
Andrii Perepichay³, Odarka Prokhorenko³

¹ China-Ukraine Institute of Welding, Guangdong Academy of Sciences, Guangdong Provincial Key Laboratory of Material Joining and Advanced Manufacturing, Guangzhou, 510650, China

² E.O. Paton Electric Welding Institute, National Academy of Sciences of Ukraine, Kazymyr Malevych Str., 11, 03150 Kyiv, Ukraine

³ National Technical University of Ukraine, Igor Sikorsky Kyiv Polytechnic Institute, 37, Peremohy Ave, 03056 Kyiv, Ukraine

* Corresponding author's e-mail: zhaoyq@gwi.gd.cn

ABSTRACT

Assessment of the residual stress-strain state (SSS) at MIG welding of aluminium alloys structures is relevant, because of the need to predict formation of residual stresses and strains, which may lead to lowering of fatigue strength of such a structure. Therefore, the research is devoted to determination of the influence of the mode of pulse-arc (MIG) welding of 1561 aluminium alloy of Al-Mg-Mn system (4 mm thickness) on the thermal cycle of the process and prediction of the influence of rigid restraint of the welded specimens in the assembly-welding fixture on the residual SSS of butt and tee welded joints. For this purpose, a finite element model of calculation of the temperature fields and SSS was created on the base of the conducted technological studies, which ensured up to 10% accuracy, that is an acceptable result for technological calculations. This model was used to determine the longitudinal and transverse tensile stresses and displacements, equivalent strains and stresses, out-of-plane displacements of the welded joint of Al-Mg-Mn aluminium alloy. It was found that rigid restraint of the specimens leads to formation of maximal equivalent stresses at MIG welding: for the butt joint – up to 190 MPa, forming in the points of transition from the weld to the base metal on the face surface; for the tee joint – ~250–260 MPa, forming in the weld area in the flange. Out-of-plane displacement after unfastening of the welded specimens from the assembly-welding fixture was equal to: for butt joint – up to 0.1 mm; for tee joint – up to formation of a plastic zone in the flange ~1.7 times larger than in the web, and out-of-plane bending of the web by 1.31 mm.

Keywords: aluminium alloy, MIG will welding (consumable electrode arc), butt and tee joints, modes, temperature distribution, residual stresses, strains.

INTRODUCTION

When welding aluminium alloy structures, one of the most important aspects is evaluation of the residual stress-strain state (SSS). So, in research [1–3] it is noted that in welding it is necessary to take into account the influence of material nonlinearity, geometrical nonlinearity and work hardening on the welding process, as well

as the difference in the welding temperature field, residual stresses and welding strains. Methods of mathematical simulation of thermal processes are applied for prediction of physical-metallurgical processes and thermal cycles in the processes of fusion welding and in related technologies [4–9], and for distribution of residual stresses and welding strains it is rational to use numerical modeling by finite element method, which is in good

agreement with experimentally measured data [10, 11]. At the same time, sufficient accuracy of technological calculations is considered to be no worse than 10–15% [12–14]. Predominantly butt joints are considered in the examples of such prediction [15, 16]. However, other kinds of joints, in particular, tee joints, are also of interest [17, 18].

In research [19] it is shown that at MIG welding of 8 mm plates from 5083-H321 alloy, the peak value of transverse stresses varies from +50 MPa (19% of the strength of the plate base metal) at the HAZ boundary up to –150 MPa (57% of strength) on the weld central line. Equivalent values for longitudinal stresses are equal to +90 MPa (34% of strength) at the distance of approximately 22 mm from the weld central line up to –120 MPa (45% of strength) on the weld central line. The residual stress-strain state and mechanical properties of aluminium alloy joints produced by MIG welding are also influenced by weld geometry, in particular reinforcement size [20], as well as the welding sequence, particularly, for tee joints [21].

Residual stresses in fusion welding of aluminium alloys are quite significant and higher than those arising in welding processes without fusion, for instance in friction stir welding [22], or plastic strain welding [23]. It is proposed to lower the significant residual stresses, arising in aluminium alloy welding, by postweld treatment, for instance shot blasting [24], preheating and/or postweld heat treatment [25]. It should be noted that the occurrence and development of residual stresses can lead to the destruction of the welded joint [26]. In this case, the deformations can be assessed by studying the topography of the fracture surface [27].

One of the approaches to reduce the residual stresses and strains in MIG welding of aluminium alloys can be an increase of the locality of thermal impact, through application of pulse modulation of welding current [28, 29]. In research [30] the thermoelastic-plastic model was used to conduct 3D finite element modeling of temperature, residual stresses, and strain fields of the weld in a 6061-T6 tee-joint during double pulse MIG welding (DP-MIG). It was found that stresses reach 273 MPa in the fusion zone that causes angular distortion of 1.61°.

Thus, at MIG welding of aluminium alloys one of the main drawbacks is the risk of formation of considerable residual strains and development of stresses, which may lead to lowering of the welded structure fatigue strength [31]. It is

especially important to take into account residual deformations and stresses when manufacturing critical welded structures [32–35]. For prediction of the residual stress-strain state, it is necessary to model the temperature field of the respective welded structure. One of the approaches to simplification of such a modeling task is breaking up the structure into spatial primitives such as butt and tee joints, and prediction of the residual stress-strain state for them by modeling the temperature fields.

PURPOSE, MATERIALS AND METHODS

The objective of the research is to establish the influence of the mode of MIG welding of an aluminium alloy of Al-Mg-Mn system on the process thermal cycle and to predict the influence of rigid restraint of the welded specimens in the assembly-welding fixture on the residual stress-strain state of the butt and tee welded joints.

The following tasks will be addressed to achieve the defined objective:

- conduct technological experiments, study the distribution of thermal field and strains in the butt and tee joints of 1561 aluminium alloy, produced by MIG welding;
- create a model of predictive calculation of thermal fields, residual stresses and strains and perform its validation;
- determine the thermal fields, residual stresses and strains for butt and tee joints of 1561 aluminium alloy, produced by MIG welding;
- determine the main tendencies and regularities of the influence of assembly-welding fixture on the results of MIG welding of butt and tee joints of 1561 aluminium alloy.

To conduct the technological experiments 1561 aluminium alloy of Al-Mg-Mn system was selected as the base metal (Table 1), which has the strength (static fracture resistance) of not less than 360 MPa and relative elongation of the order of 11%. This material was used to produce plates of 290 × 100 × 4 mm size, from which 12 butt joints and 12 T-joints were welded. ER5356 wire of 1.2 mm diameter was selected as electrode wire (Table 1). When conducting experimental studies, the results were averaged for at least 6 specimens. MIG welding was conducted in the atmosphere of higher grade argon of 99.993 vol.% purity. The geometry diagram of the welded joints is shown

Table 1. Chemical composition of materials used in the investigations

Material	Chemical element, wt. %									
	Al	Mg	Mn	Si	Fe	Cu	Zn	Zr	Cr	Ti
Base metal 1561	Base	5.5–6.5	0.7–1.1	≤0.4	≤0.4	≤0.1	≤0.2	0.02–0.12	-	-
Welding wire ER5356	Base	4.5–5.5	0.1–0.2	-	-	-	-	-	0.05–0.20	0.06–0.20

Note: alloy 1561 does not have an international standard (standard GOST 17232-99 “Plates made of aluminum and aluminum alloys”); wire ER5356 – EN ISO 18273:2015, IDT.

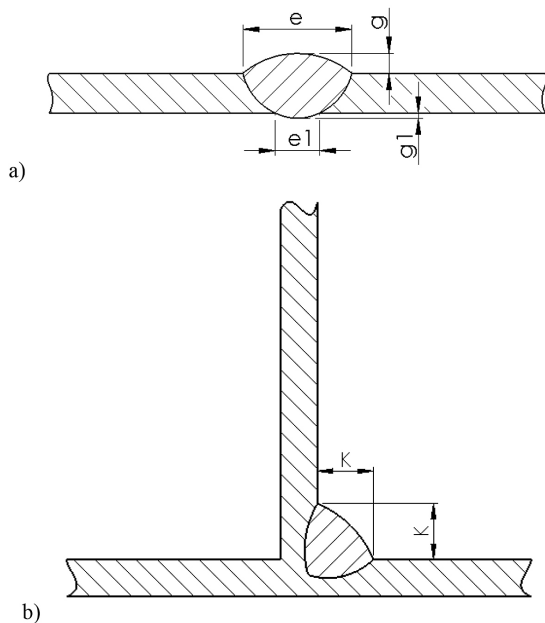


Figure 1. Schemes of welded joints:
(a) – butt; (b) – T-joint

in Figure 1. Investigations were conducted by the following procedure: specimen preparation for welding (mechanical cutting out of the specimens from the sheet so that welding took place along the rolling bands, chemical etching of the specimens to eliminate contaminations and to reduce the oxide film); assembly of the butt and tee joints in the assembly-welding fixture, mounting thermocouples at the beginning and end of the joint; mode selection by the criterion of sound weld formation and performance of MIG welding, preparation of macrosections, accumulation of experimental data; development of a model for finite element modeling, conducting modeling of temperature field distribution, model validation; prediction of residual stresses and strains using finite element modeling; measurement of residual strains, model validation; analysis of the obtained results.

A laboratory facility was designed and manufactured for technological studies. It consists of (Fig. 2): assembly-welding fixture which allows clamping the specimens for welding butt and tee

joints (Fig. 2a, b); three-coordinate manipulator and anthropomorphic robot-manipulator for fastening and movement of the welding torch (Fig. 2,c); power source with wire feed mechanism are designed for up to 400 A welding current.

For MIG-welding the specimens were first chemically etched (in NaOH and HNO₃ with water rinsing), which was followed by their clamping in the assembly-welding fixture with simultaneous connection of three thermocouples in the specimen middle and at the distance of 70–80 mm from its edges (Fig. 3). The thus prepared specimens were welded in the respective modes.

The method of metallographic analysis [36–42] was used to study the structure of the produced welds. Residual welding displacement (deformation) in butt joint specimens was determined by the method of comparison of the measured sagging of the blanks in the initial condition with welded joint sagging [43–45]. Measurements were conducted on the surface of the test plate by a dial indicator with a division value of 0.01 mm (Fig. 4a). Residual displacements in the tee joint specimens were determined using the same equipment by a similar procedure. The flange was fastened by press-down plates to measure the web bending away from the vertical (Fig. 4b).

INVESTIGATION RESULTS

Results of conducting the technological studies

Selection of the parameters of the modes of MIG welding of butt and tee joints of 1561 alloy were conducted by the following criteria: presence of guaranteed complete penetration of butt specimens and partial penetration of the flange and web of the tee specimens, absence of undercuts, presence of a smooth transition from the deposited to base metal, reliability of gas shielding, and minimizing the heat input. The mode parameters selected as a result are shown in Table 2, and dimensions

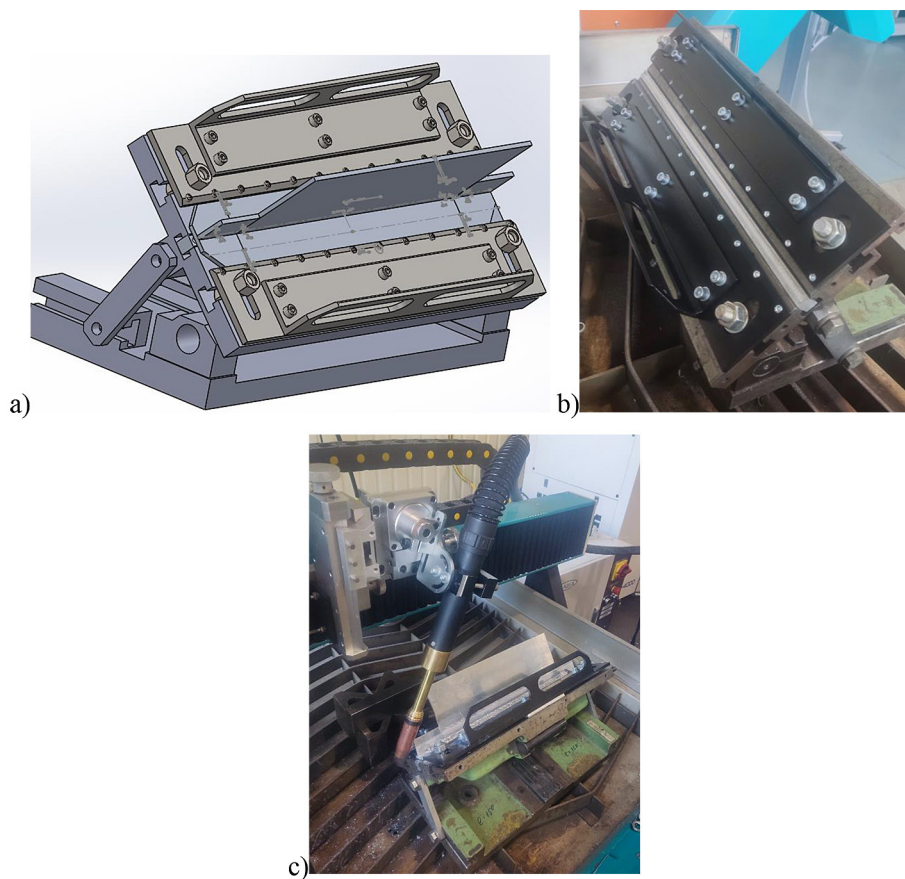


Figure 2. Laboratory facility for conducting the technological studies: (a), (b) – 3D-model and appearance of assembly-welding fixture for making butt and tee joints; (c) – appearance of a three-coordinate manipulator with a MIG-welding torch and mounted assembly-welding fixture

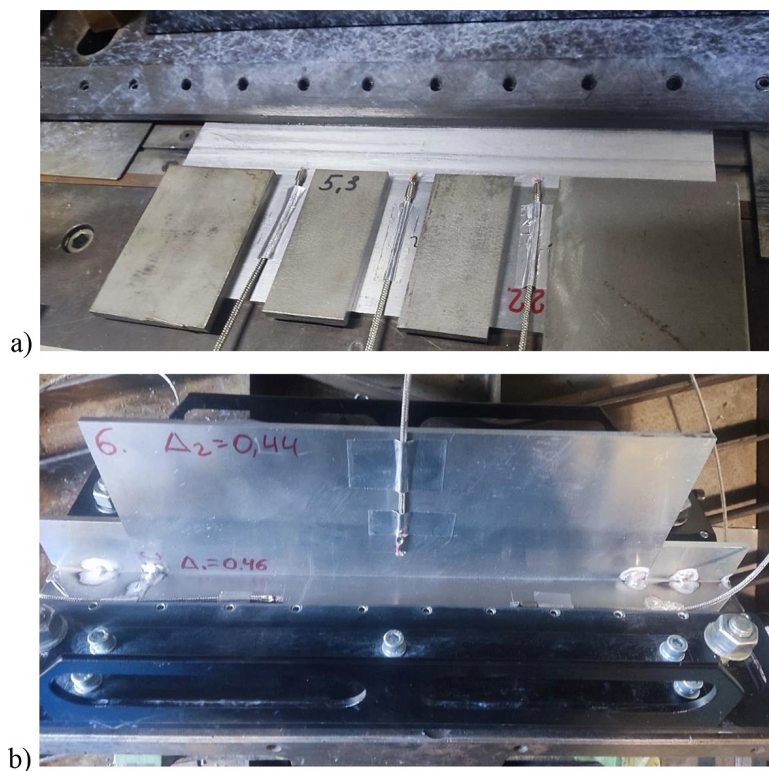


Figure 3. Assembly of specimens of 1561 alloy for MIG-welding with thermocouple mounting



a)



b)

Figure 4. Measurements of residual welding displacements (deformations) in specimens of butt (a) and tee (b) welded joints

Table 2. Parameters of the modes of MIG welding of specimens of butt and tee joints of 1561 alloy

Specimen type	Wire feed rate V_{wire} , m/min	Welding current I , A	Arc voltage U , V	Welding speed, V , mm/min	Shielding gas flow rate Q , l/min	Heat input E , J/mm
Butt	6.9	125	19.5	380	24	347
Tee	9.4	153	16	400	16	330

Note: heat input E was determined allowing for process efficiency $\eta=0.9$ [46].

of the produced weld and weld pool, required for further modeling of the stress-strain state are given in Table 3. Appearance and macrosections of the produced specimens are given in Fig. 5. The parameters of the obtained welds were checked according to the ISO 10042 standard and they met the requirements of the standard. The convexity of the butt joint weld corresponds to quality level C and is very close to the requirements of level B. The convexity of the root part of the weld corresponds

to level B. The convexity of the T-joint weld corresponds to the requirements of quality level B. During welding, the thermal cycles were recorded by thermocouples mounted on the specimens that will be described in greater detail below.

Welding was performed in the “1F” position, as the most favorable position for the welding process. In this position, gravity facilitates the transfer of electrode metal. When welding T-joints in this position, the uniformity of the weld leg formation

Table 3. Geometrical dimensions of the weld and weld pool of specimens of butt and tee joints of 1561 alloy

Specimen type	Weld width e , mm	Weld width from the reverse side $e1$, mm	Weld reinforcement g , mm	Weld reinforcement from the reverse side $g1$, mm	Weld leg, K , mm	Weld pool length L , mm	Length of weld pool frontal part L_f , mm
Butt	11	4	2.9	2	-	10	5.2
Tee	-	-	-	-	6	9	4

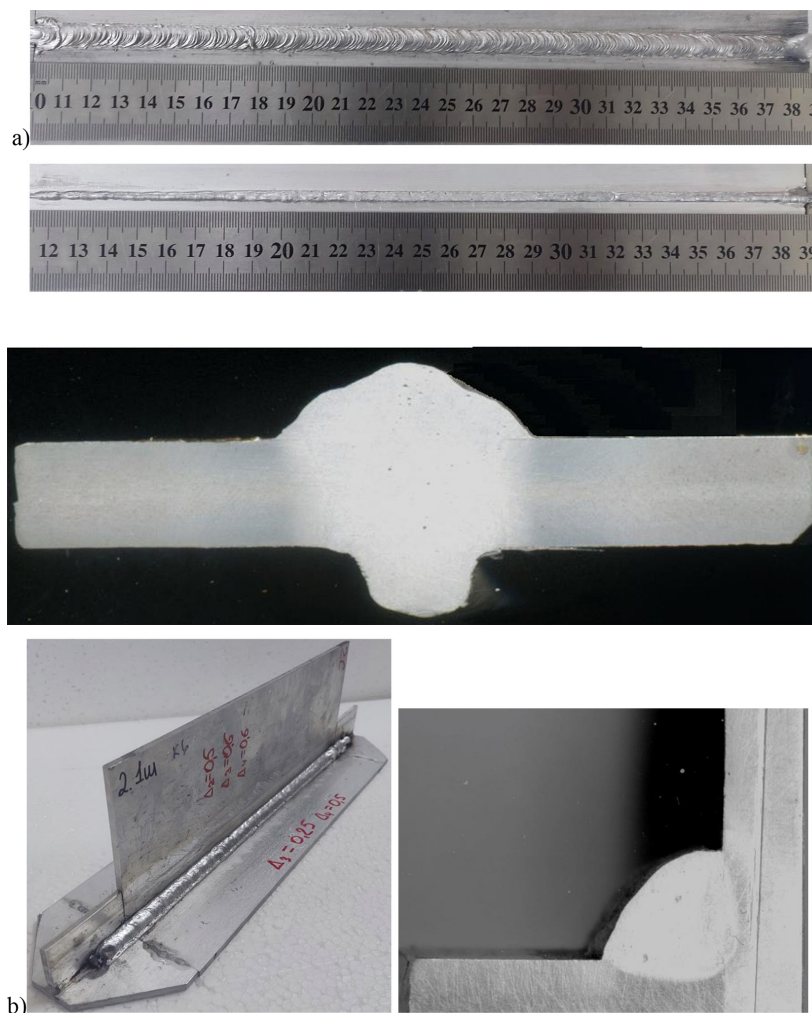


Figure 5. Appearance and cross-sections of butt (a) and tee (b) welded joints of 1561 alloy

is improved. This also reduces the likelihood of burning through the wall or flange of the joint. In general, this position is preferable when performing T-joints of long welded structures in production.

Creation and verification of the model for calculation of the temperature fields, residual stresses and strains

At mathematical modeling of MIG welding process the available experience was taken into account [47–49]. Modeling of thermal processes at MIG welding of 1561 alloy was performed by

finite element method [50] at different configurations of welding parameters.

In this study Simufact Welding software environment, which specializes on simulation of welding processes in complex thermo-elasto-plastic definition, was used. The main advantage of Simufact Welding consists in the possibility of assigning a wide range of welding modes and modeling materials with nonlinear deformation laws, which ensures greater correspondence to the real welding conditions. For realistic reproduction of the local physical processes Simufact Welding applies adaptive refinement of the mesh

in the weld zone and allows assigning different conditions of part fastening that ensures more precise modeling of the thermal deformation state during welding. It allows tracking abrupt temperature gradients and development of plastic zones, forming directly during welding.

Moreover, Simufact Welding realizes a number of specialized models of the welding heat source, among which the double ellipsoid model proposed by J. Goldak was selected [51]. In this model J. Goldak sets the normal (Gaussian) distribution of heat source power density in the volume of a body having the shape of a double ellipsoid [52]. Temperature field $T(x,y,z,t)$ of such a distributed volumetric heat source is described by a differential nonlinear heat conductivity equation in any point of the body:

$$c\rho \frac{\partial T}{\partial t} = \frac{\partial}{\partial x} \left(\lambda \frac{\partial T}{\partial x} \right) + \frac{\partial}{\partial y} \left(\lambda \frac{\partial T}{\partial y} \right) + \frac{\partial}{\partial z} \left(\lambda \frac{\partial T}{\partial z} \right) + q_{vol} \quad (1)$$

where: $q_{vol}(x,y,z)$ is the volume fraction of the source thermal power, W/cm³; c is the thermal diffusivity, ρ is the density, λ is the heat conductivity of 1561 alloy.

Within the double ellipsoid model the volumetric density of the source thermal power $q_{vol}(x,y,z)$ has a normal (Gaussian) distribution. Then, in keeping with the normal distribution law for the frontal (at $x \geq 0$) and tail (at $x < 0$) parts of the ellipsoid, we can write:

$$q_{vol,f} = q_{max} e^{(-A_1x^2 - By^2 - Cz^2)} \quad (2)$$

$$q_{vol,r} = q_{max} e^{(-A_2x^2 - By^2 - Cz^2)} \quad (3)$$

where: q_{max} is the maximal thermal power in the ellipsoid center; A_1, A_2, B, C are the coefficients of distribution concentration in the positive and negative direction along axis OX and along axes OY and OZ , respectively; f and r are the coefficients of the ellipsoid frontal and tail parts.

As the source effective thermal power Q (for arc welding $Q = \eta IU$) is assigned by both the components of volumetric power density $q_{vol,f}$ and $q_{vol,r}$, we can write:

$$Q = \int_0^\infty \int_{-\infty}^\infty \int_{-\infty}^\infty q_{max} e^{(-A_1x^2 - By^2 - Cz^2)} dx dy dz + \int_{-\infty}^0 \int_{-\infty}^\infty \int_{-\infty}^\infty q_{max} e^{(-A_2x^2 - By^2 - Cz^2)} dx dy dz \quad (4)$$

Allowing for standard integral function $\int_0^\infty e^{-ax^2} dx = \frac{\sqrt{\pi}}{2a}$ $a > 0$, we obtain from (4):

$$Q = 2q_{max} \frac{\sqrt{\pi}}{2\sqrt{A_1}} \frac{\sqrt{\pi}}{2\sqrt{B}} \frac{\sqrt{\pi}}{2\sqrt{C}} + 2q_{max} \frac{\sqrt{\pi}}{2\sqrt{A_2}} \frac{\sqrt{\pi}}{2\sqrt{B}} \frac{\sqrt{\pi}}{2\sqrt{C}} = q_{max} \left(\frac{\sqrt{\pi^3}}{4\sqrt{A_1BC}} + \frac{\sqrt{\pi^3}}{4\sqrt{A_2BC}} \right) \quad (5)$$

Hence,

$$q_{max} = 4Q \left(\frac{\sqrt{A_1A_2BC}}{\sqrt{\pi^3(\sqrt{A_1} + \sqrt{A_2})}} \right) \quad (6)$$

In keeping with [51] normally distributed functions $q_{vol,f}$ and $q_{vol,r}$ will decrease to $0.05q_{max}$ value at certain distances a_f, a_r, b and c from the origin of coordinates of a moving system connected to the double ellipsoid heat source, then:

$$\begin{aligned} q_{vol,f}(x = a_f, y = 0, z = 0) &= \\ q_{vol,r}(x = -a_f, y = 0, z = 0) &= 0.05q_{max} \\ q_{vol,f,r}(x = 0, y = b, z = 0) &= \\ q_{vol,f,r}(x = 0, y = b, z = -c) &= 0.05q_{max} \end{aligned} \quad (7)$$

Substituting (7) into (2) and (3) we will determine A_1, A_2, B, C :

$$\begin{aligned} A_1 = \frac{-\ln 0.05}{a_f^2} \approx \frac{3}{a_f^2}; \quad A_2 = \frac{-\ln 0.05}{a_r^2} \approx \frac{3}{a_r^2} \\ B = \frac{-\ln 0.05}{b^2} \approx \frac{3}{b^2}; \quad C = \frac{-\ln 0.05}{c^2} \approx \frac{3}{c^2} \end{aligned} \quad (8)$$

Substituting Equations 6 and 8 into Equations 2 and 3, and having made the transition from the moving coordinate system to the general one, we will obtain the following equation:

$$q_{vol,f} = f_f \frac{6\sqrt{3Q}}{a_f b c \pi^{3/2}} e^{-3 \left[\left(\frac{x+v(\tau-t)}{a_f} \right)^2 + \left(\frac{y}{b} \right)^2 + \left(\frac{z}{c} \right)^2 \right]} \quad (9)$$

$$q_{vol,r} = f_r \frac{6\sqrt{3Q}}{a_r b c \pi^{3/2}} e^{-3 \left[\left(\frac{x+v(\tau-t)}{a_r} \right)^2 + \left(\frac{y}{b} \right)^2 + \left(\frac{z}{c} \right)^2 \right]} \quad (10)$$

where: τ is the time elapsed since the start of the heat source action; t is the current time; v is the speed of the source movement (welding speed); x, y, z are the ellipsoid half-axes in coordinate directions OX, OY, OZ ; f_f and f_r are the coefficients which determine the ratio of the heat, added to the ellipsoid frontal and tail parts ($f_f=0.4, f_r=1.6$ [51]).

Application of this model in Simufact Welding environment enables at each stage (heating, melting, cooling) following the dynamics of the temperature field formation, assessing the magnitude and distribution of the residual stresses, as well as determination of the magnitude

of plastic deformations. It resulted in forming a comprehensive understanding of the dynamics of MIG welding process, which allowed correct comparison of the numerical modeling results with experimental observations.

The geometrical and finite element models were constructed using Visual Mesh software package, while further calculations were performed in Simufact Welding environment [10, 19]. In order to reproduce the real conditions of rigid restraint, not only the plates and the weld, but also the fixture elements (backing, press-down plates) were modeled. Assigning the boundary conditions consisted in fixing the movement of the assemblies, coming into contact with the fixture, to simulate absence of deformations in the fastened zone.

2D-section of the plate and the weld was first created, which was later stretched into the third dimension, forming a 3D model. The mesh

consisted of predominantly four node tetrahedral and eight node hexahedral elements (0.1–0.2 mm in the vicinity of the weld, 0.5–3.0 mm farther from the weld), where the action of mobile spatial heat source was calculated (9)–(10) (Fig. 6). Sensitivity analysis showed that further refinement of the element size in the fusion zone, even though it improves the accuracy (by 1–2% on average), greatly increases the calculation time that is in agreement with the conclusions of works [50, 51]. An optimal content of elements in the models was 13–15 thous., that ensured an acceptable accuracy for evaluation of the residual stresses and strains.

Temperature-dependence physico-mechanical characteristics of the alloy and the filler material were entered on the base of tabulated data and our own experimental measurements [4, 10]. Plastic deformation was determined on the base of «stress-strain» curves, corresponding to

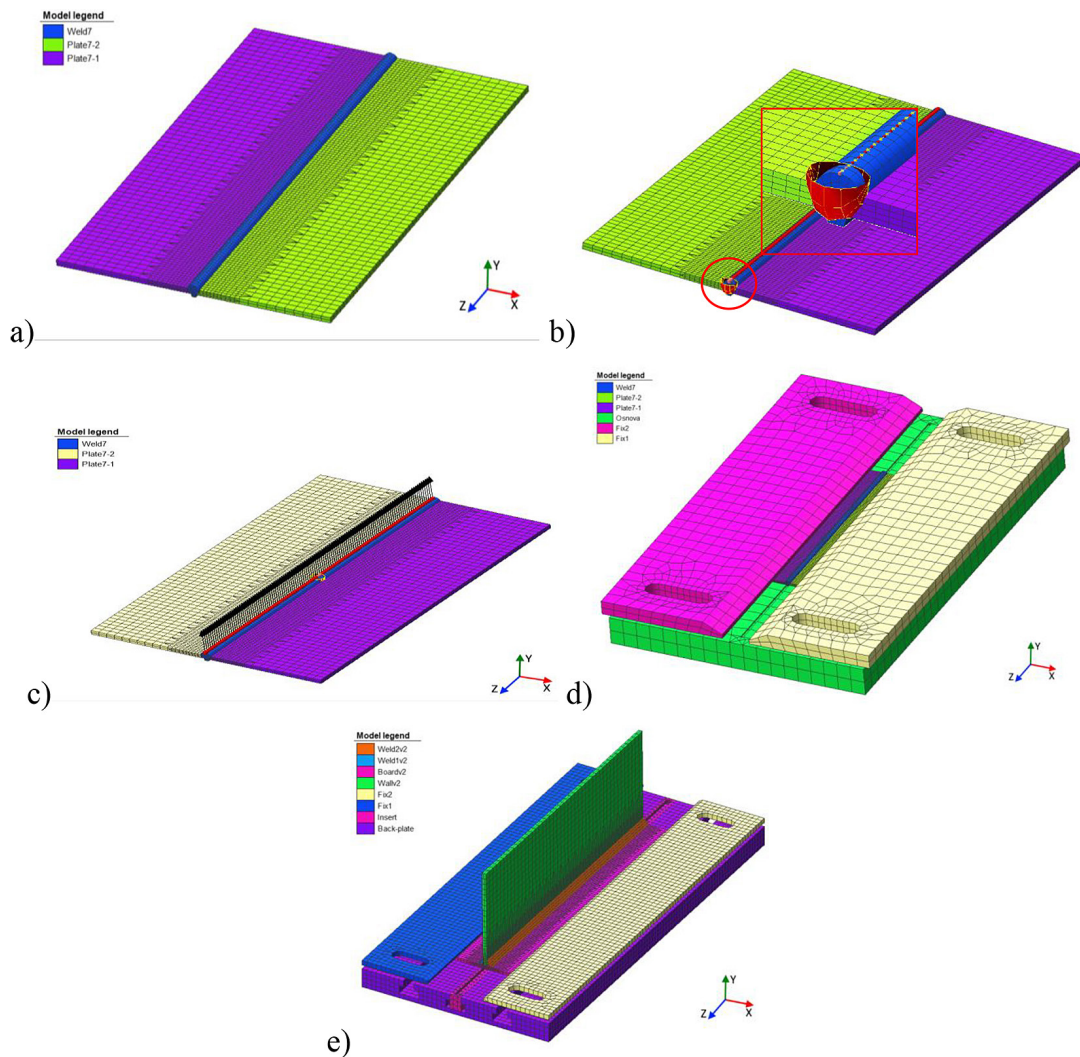


Figure 6. Finite element 3D models of a butt joint (a) and spatial position of the heat source (b) during its welding; of a tee joint (c), of butt (d) and tee (e) joints with a substrate and fixture

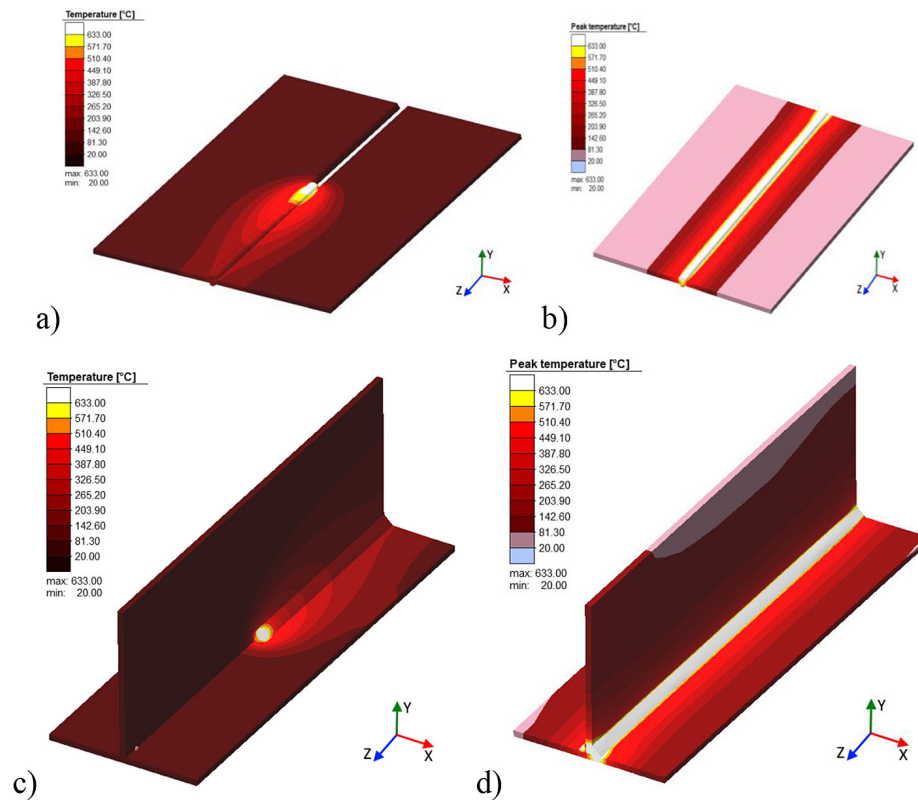


Figure 7. Temperature field at the moment of the welding arc reaching the middle of the weld length (a,c) and peak temperatures (b, d) in the butt (a, b) and tee (c, d) welded joints

different temperature ranges and strain rates. Allowing for the rigid restraint of the plates in the assembly-welding fixture, the model realized restriction of the degrees of freedom at the contacts with the backing and the press-down plates. After construction of the geometry and the mesh the model was exported to Simufact Welding, where calculations were performed in the thermo-elasto-plastic definition.

Validation of the developed finite element model was performed by comparing the thermal cycles, obtained in the experiment using thermocouples and as a result of numerical calculation (Fig. 7). Comparison of the model and experimental thermal cycles is shown in Fig. 8. One can see from this comparison that the created finite element model allows prediction of the results of aluminium alloy MIG welding with an accuracy not worse than 5%.

Analysis of the parameters of residual stress-strain state (SSS) of a butt welded joint

Calculation of the parameters of residual SSS for a symmetrical butt joint of $290 \times 200 \times 4$ mm size was performed for the process of welding

and cooling in the assembly-welding fixture, which had the form of two solid plates (Fig. 6d), placed on 40 mm base relative to the weld, which provided rigid restraint of the welded plate in the plane. After unfastening the welded joint from the fixture, the level of residual stresses in the weld area decreases to ~ 150 MPa with formation of compressive stresses outside of the plastic strain zone of the order of -68 MPa with further lowering to ~ -40 MPa at the edges (Fig. 9a).

Fields of transverse normal stresses by their magnitude are by an order smaller than the longitudinal normal stresses (Fig. 9b). The near-end areas at the weld start and end are compressed, on the face surface the stress value is not higher than ~ -10 MPa in the zone restrained during welding; in the zone free from the fixture the stresses reach ~ -30 MPa, because of impossibility of free expansion during welding.

The main cause for formation of residual welding stresses are the uncompensated residual plastic strains, which are non-uniformly distributed in the welded joint cross-section. Figure 10a shows the field of residual equivalent plastic von Mises strains with removed fixture [53]: areas with zero strain values in the regions of contact of

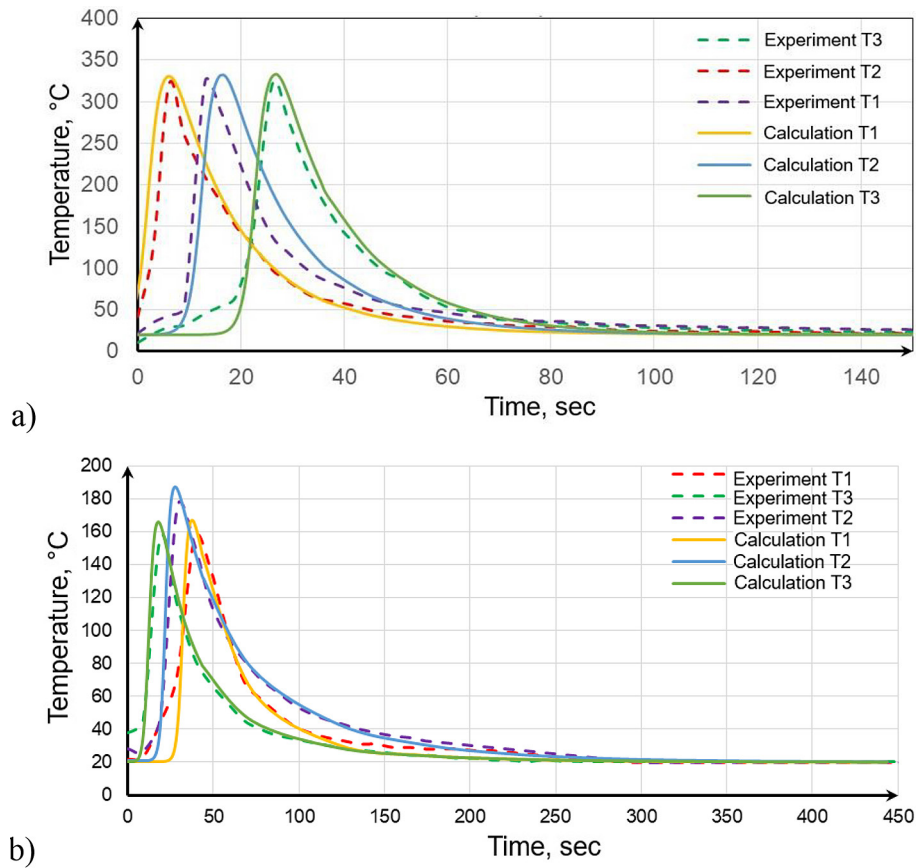


Figure 8. Thermal cycles of the experimental and modeled process of welding the butt (a) and tee (b) joints

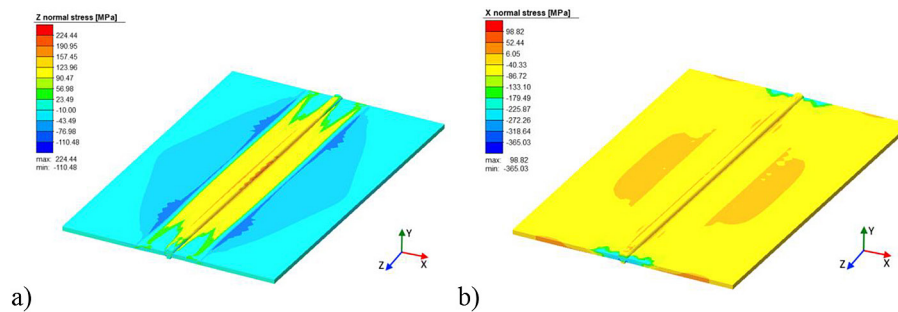


Figure 9. Fields of residual longitudinal (a) and transverse (b) stresses

the fixture with the plates are clearly defined. The central area of the welded joint heated up to high temperature, which is free from the fixture during welding, is characterized by rather abrupt increase of plastic strains with a maximum at the boundary of the fixture action. The limits of the zone, where plastic strains develop, are the same on the left and on the right of the weld axis due to the welded joint symmetry, and they are equal to 33 mm each, which is 1.65 times larger than the fastening base during welding (40 mm) by. Such a width of plastic zones is attributable to the action of the fixture during welding, which prevents free expansion of

the plates being welded in the transverse direction and promotes development of plastic strains.

Maximal values of von Mises equivalent stresses are concentrated in the weld and near-end areas at the weld start and end (Fig. 10b) [53]. In the joint central part the value of stresses decreases nonuniformly, with peak overshoots on the boundaries of action of the press-down plates and boundaries of the plastic strain zone. Maximal stress values are in place on the weld axis (up to ~180 MPa) and in the places of transition from the weld to the base metal (up to 190 MPa), that is ~30% less than the deposited metal ultimate

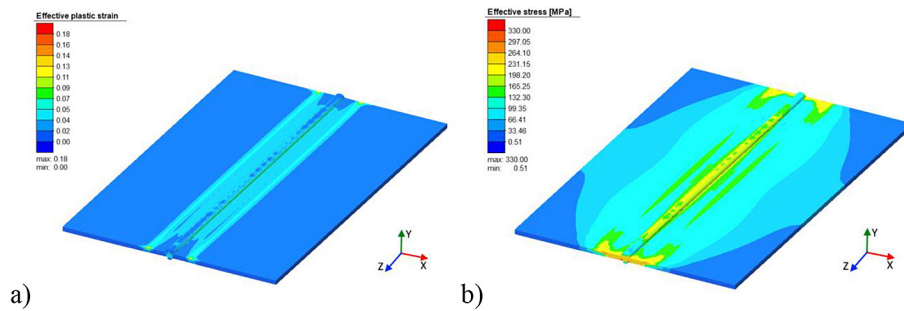


Figure 10. Field of residual von Mises equivalent plastic strains (a) and stresses (b)

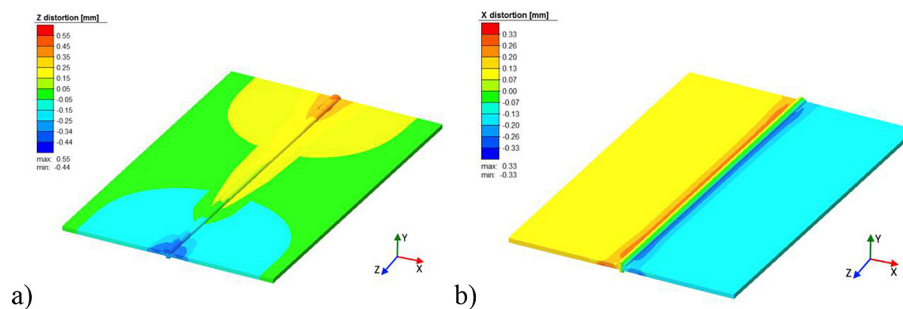


Figure 11. Fields of residual longitudinal (a) and transverse (b) displacements in the butt joint

strength. Joint removal from the fixture after welding led to maximal shortening of the weld start (~ 0.37 mm) and end (~ 0.43 mm) (Fig. 11a). Across the welded joint width the longitudinal shrinkage is nonuniformly distributed: the central part had the largest shrinkage displacements as a result of the influence of the high-gradient temperature field of the welding arc on it. The area of maximal displacements corresponds to the base of fastening the plates being welded. The fields of transverse displacements after the fixture removal (Fig. 11b) demonstrate practically uniform (~ 0.3 m) transverse shortening of the welded joint along the entire weld length. Maximal magnitude of out-of-plane displacements of the welded plates, after freeing them from the rigid restraint, is equal to ~ 0.16 mm on the weld axis (Fig. 12). In the joint areas which were in contact with the fixture during welding, displacements can be considered zero (~ 0.0007 mm). Displacements are uniformly distributed along the weld length, except for edge areas, where they reach ~ 0.3 mm.

Analysis of the parameters of residual stress-strain state (SSS) of a tee welded joint

Calculation of the parameters of the residual SSS for a model of a symmetrical tee joint was performed at the action of assembly-welding

fixture in the form of two solid plates, placed on the base of 60 mm as to the fillet welded joints. Press-down plates rigidly fixed the tee flange in the plane at welding fillet welds in the gravity position and during cooling.

The general pattern of distribution of the residual longitudinal stresses in the welded tee joint after its unfastening from the fixture is as follows (Fig. 13a): the flange is in tension, because of application of the restraining fixture during welding. In the web the stresses are distributed in a classical manner: tensile stresses act in the plastic zone, and compressive stresses act in the reactive zone. The pattern of distribution of the residual transverse stresses along the weld length in the tee joint corresponds to the theory of stresses and strains (Fig. 13b): tension – in the weld central part and compression – in the near-end areas.

Field of residual equivalent plastic strains in the tee joint with removed fixture has clearly defined areas with zero values of strains in the regions of the fixture contact with the plates (Fig. 14a). Welded joint areas heated up to high temperatures, free from the fixture during welding, are characterized by a rather abrupt increase of plastic strains with achievement of a maximum on the weld axis. Comparison of the width of plastic zones, which formed during welding in the tee joint flange and web, showed that rigid restraint

of the flange promotes formation of a plastic zone which is ~1.7 times larger than that in the web.

Investigations of equivalent stresses in a tee welded joint showed (Fig. 14b), that equivalent stresses of the largest magnitude of ~255 MPa formed in the weld area with their further decrease

in the flange to ~147 MPa and in the web to ~70 MPa. The difference in the magnitude of equivalent stresses in the flange and the web beyond the weld area is due to the formed field of equivalent plastic strains (Fig. 14a), the magnitude of which was influenced by the use of a fixture for the flange

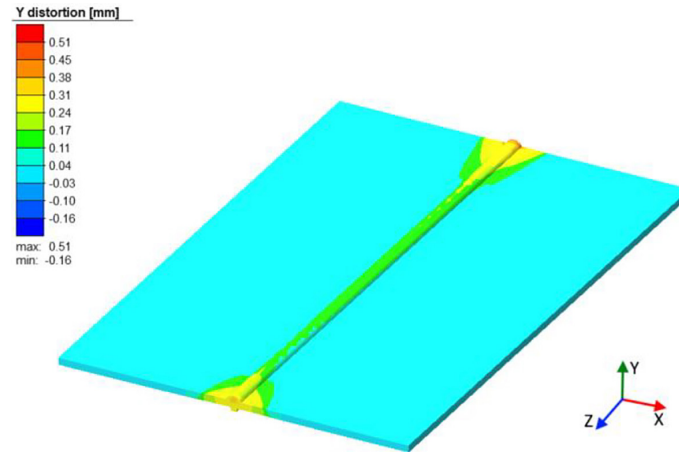


Figure 12. Fields of residual out-of-plane displacements

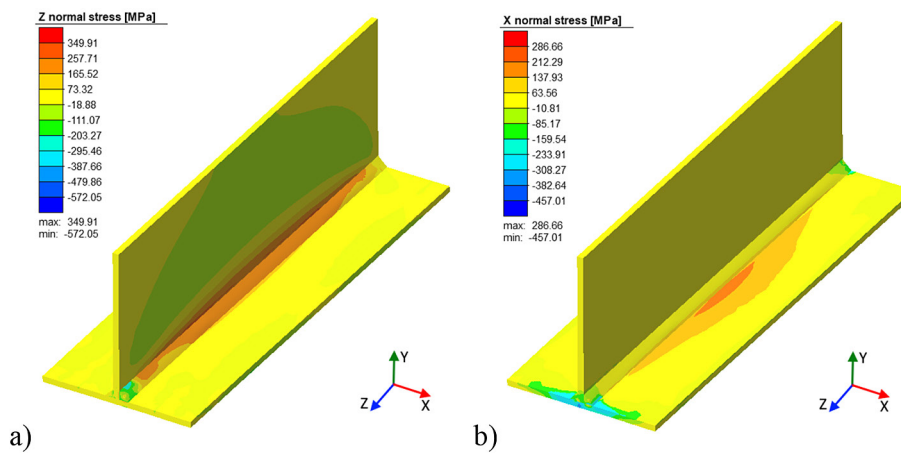


Figure 13. Fields of residual longitudinal (a) and transverse (b) stresses in the tee welded joint

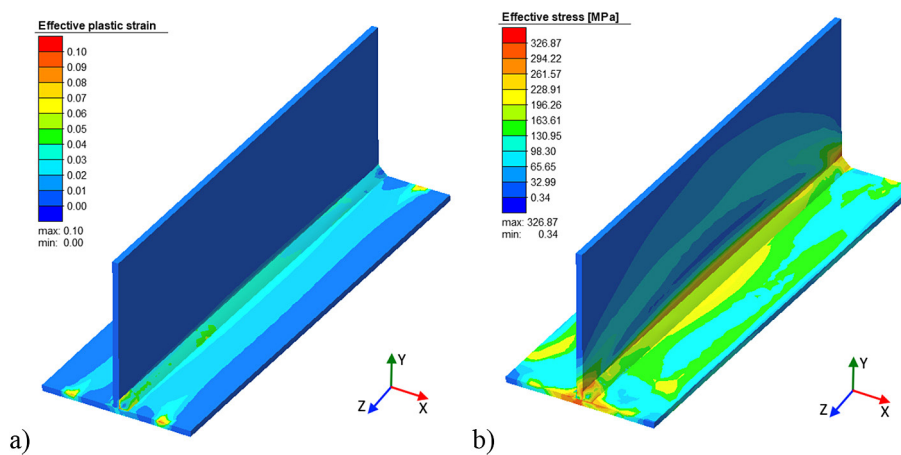


Figure 14. Field of von Mises residual equivalent plastic strains (a) and stresses (b)

fastening during welding. Residual longitudinal shortening of the tee welded joint after its releasing from the fixture was equal to ~ 0.6 mm (Fig. 15a). Releasing from the fixture after welding led to maximal shortening of the weld start and end, which is related to longitudinal shrinkage of the weld metal. The transverse displacement fields after the fixture removal allow to be sure of practically uniform transverse shortening of the flange of ~ 0.2 mm along the entire weld length (Fig. 15b). Tee web shortening in the direction transverse relative to the weld (along Y axis) is by an order smaller than that in the flange, and it is equal to ~ 0.03 mm along the entire weld length (Fig. 15c).

In the area of the flange, removed from the fixture, the magnitude of out-of-plane displacements is equal to ~ 0.15 mm with achievement of a maximum of ~ 0.32 mm in the weld area (Fig. 16). In the areas of contact of the plates being welded with the fixture the displacements are minimal at ~ -0.01 mm. Maximal out-of-plane displacements formed in the web, in the point farthest from the weld, because of absence of fastening during welding: deviations from the vertical by ~ 1.33 mm. At the flange ends the residual displacements are small and equal to ~ 0.09 mm for both the sides, due to the influence of the fixture during welding and cooling.

DISCUSSION OF INVESTIGATION RESULTS

Conducted calculation studies showed that for butt joints of 1561 alloy specimens:

- magnitudes of longitudinal stresses on the joint face side on the weld axis are 12% lower than those on the reverse side, magnitudes of longitudinal stresses in the points of transition from the weld to the base metal are peak values, but

their magnitude is lower than the weld metal ultimate strength on the joint face side by $\sim 33\%$, and on the reverse side by $\sim 68\%$;

- along the weld length the magnitude of transverse stresses on the face and reverse surfaces is approximately the same, which is indicative of uniform transverse shrinkage of the weld metal during cooling in the fixture;
- equivalent plastic strains on the joint reverse side are up to ~ 2.5 times higher than the strains on the face side, here equivalent stresses on the face side are up to $\sim 10\%$ higher than those on the reverse side;
- after unfastening from the fixture, the residual values of longitudinal shortening on the face surface exceed similar values for the reverse surface by up to 10%.

In the HAZ the nature of out-of-plane displacements is the same on both sides of the joint, and their magnitude is up to 30% higher on the reverse surface, on the weld axis the displacements are 40–45% greater on the welded joint face side, the nature of distribution and magnitude of transverse shortening on the welded joint reverse side are practically identical to the pattern of their distribution on the joint face side. For tee joint of 1561 alloy specimens:

- in the area of contact of the web with the flange the level of longitudinal tensile stresses is approximately the same for the face and the reverse sides;
- magnitude of transverse stresses in the web and the flange on the face side is 25–35% smaller than on the reverse side;
- distribution of equivalent plastic strains in the flange and the web for the face and the reverse surfaces of the welded joint is practically identical, except for points, belonging to the weld

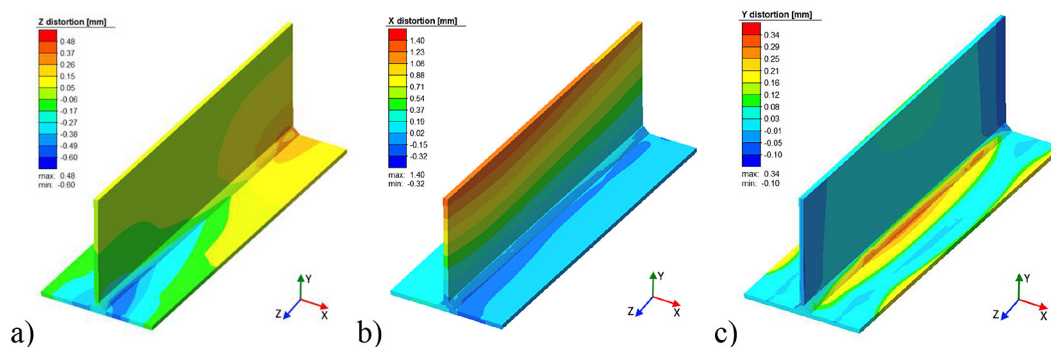


Figure 15. Fields of residual longitudinal (a) and transverse (flange – along axis X (b), web – along axis Y(c)) displacements in the tee welded joint

area; on the weld face surface the peak strain values are ~4 times greater than those on the reverse side;

- equivalent stresses on the flange face surface are 40% higher than those on the reverse surface;
- longitudinal displacements along the weld length after unfastening from the fixture are 14–58% smaller than on the reverse side;
- transverse shortening on the flange face surface in the weld area is up to 20% greater than on the flange reverse side;
- nature of distribution of the displacements for the face and reverse sides, both in the flange, and in the web, is the same, magnitude of out-of-plane displacements is different in the weld area: for the face side it is 55–60% larger on the axis between the welds than for the reverse side, and in the leg area it is 13–19% larger for the face side than for the reverse side.

The conducted studies have shown that the values of residual stresses (both longitudinal and transverse), equivalent deformations and stresses, as well as longitudinal and transverse displacements, during welding of T-joints are several times greater than the analogs occurring during welding of butt joints. This is due to the fact that the linear energy of welding a butt joint is 347 J/mm, and a T-joint is 330 J/mm for each of the two seams.

The above-described comparison of the model and experimental thermal cycles (Fig. 8) showed that the developed finite element models of the butt and tee joints allow predicting the results of MIG welding of the aluminium alloy with not worse than 5% accuracy. This parameter of the model accuracy can be determined more

precisely by comparison of the results of their application to determine out-of-plane displacements after MIG welding of 1561 alloy.

Mode precise determination of the validity of prediction by the developed finite element models of the butt and tee welded joints was performed by the parameter of “out-of-plane” displacement by comparing the experimental data with the results of numerical modeling of this parameter for the above-mentioned joints. Measured residual welding out-of-plane displacement in the specimens of butt and tee joints were determined by the method of comparison of sagging of the blanks in the initial condition with welded joint sagging (Fig. 4). Results of numerical modeling of out-of-plane displacements are given in Figures 12 and 16. Respective data of measurements and calculations for the same points of the welded joints were entered into Table 4. As one can see from Table 4, the error between the calculated results and the experiment by out-of-plane displacement parameter was equal to 6.5% and 9.3% for the start and end of the butt joint weld, and 7.6% for the tee joint web. Thus, it can be assumed that the developed finite element models are valid with the accuracy of up to 10% that is an acceptable result for the technological calculations.

The practical usefulness of the obtained results is as follows. Obtained results can be used at prediction of fabrication of such welded structures from aluminium alloys as car bodies, light-weight railway cars, tanks of different type for storage and transportation of food and technological substances, building structures and parts for facing, etc. For such a prediction, it is necessary to divide the structure being designed into spatial primitives,

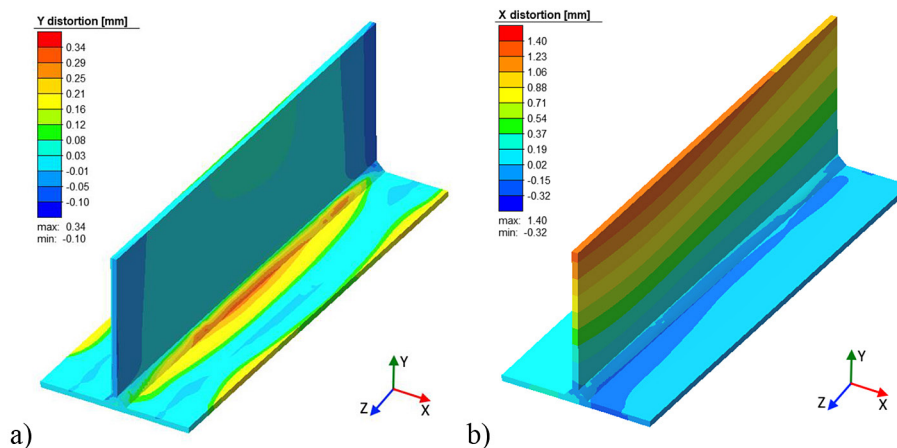


Figure 16. Fields of residual out-of-plane displacements in the tee welded joint: flange – along axis Y (a); web – along axis X(b)

Table 4. Validation of finite element (FE) models by out-of-plane displacement parameter

Butt joint of 1561 alloy						Tee joint of 1561 alloy		
Measured value of displacement of specimen points, mm		Displacement of specimen points determined by FE modeling, mm		Error, %		Measured value of specimen point displacement, mm	Specimen point displacement, obtained by FE modeling, mm	Error, %
Weld start	Weld end	Weld start	Weld end	Weld start	Weld end			
0.31	0.39	0.29	0.43	6.5	9.3	1.4	1.31	7.6

which are welded as butt and tee joints. Then the SSS for these primitives can be predicted in keeping with the developed finite element models.

CONCLUSIONS

It was established that the thermal cycle of the process of consumable electrode pulse-arc welding (MIG) of 1561 aluminium alloy of Al-Mg-Mn system depends on the process heat input and predominantly influences the specimen part near the butt, unrestrained in the assembly-welding fixture, making it rational to predict the influence of rigid restraint of the welded specimens in the assembly-welding fixture on the residual stress-strain state of the butt and tee welded joints.

The developed finite element model of calculation of the temperature fields and SSS was used to conduct the respective prediction, which allowed establishing the longitudinal and transverse tensile stresses and displacements, equivalent strains and stresses, out-of-plane displacements of the welded joint of Al-Mg-Mn aluminium alloy. The discrepancy between the calculated and experimental data is not higher than 10%.

At MIG welding of the butt joint the maximal equivalent stresses of up to 190 MPa form in the points of transition from the weld to the base metal on the face surface, and they are ~30% lower than the deposited metal ultimate strength. At welding of the tee joint the maximal equivalent stresses of ~250-260 MPa form in the flange in the weld area, and they are smaller than the deposited metal ultimate strength, which eliminates the destruction of the joint.

Application of a rigidly fastening assembly-welding fixture at MIG welding of the butt joint of 1561 aluminium alloy led to minimization of out-of-plane displacements: they were equal to less than 0.1 mm. Application of a rigid fixture for the flange in welding the tee joint led to formation

of a plastic zone in the flange ~1.7 times larger than in the web, and out-of-plane bending of the web by 1.31 mm. For industrial conditions of the welding process, it is recommended to use rigidly fastening assembly-welding fixture.

Acknowledgments

The research was funded within the following programs: National Key Research and Development Program of China (Project Number: 2023YFE0201500; the GDAS' Project of Science and Technology Development [2020GDA-SYL-20200301001], China; National Key R&D Program of China [2020YFE0205300].

REFERENCES

- Li C., Fan D., Yu X., Huang J. Residual stress and welding distortion of Al/steel butt joint by arc-assisted laser welding-brazing. *Trans. Nonferrous Met. Soc. China*, 2019; 29: 692–700. [https://doi.org/10.1016/S1003-6326\(19\)64979-4](https://doi.org/10.1016/S1003-6326(19)64979-4)
- Jing H., Yu Shi, Gang Zh., Volodymyr K., Wang-Yun Le. Minimizing defects and controlling the morphology of laser welded aluminum alloys using power modulation-based laser beam oscillation. *J. Manufacturing Processes*. 2022; 83: 49–59. <http://dx.doi.org/10.1016/j.jmapro.2022.08.031>
- Korzhyk V., Khaskin V., Grynyuk A., Ganushchak O., Peleshenko S., Konoreva O., Demianov O., Shcheretskiy V., Fialko N. Comparing features in metallurgical interaction when applying different techniques of arc and plasma surfacing of steel wire on titanium. *Eastern-European Journal of Enterprise Technologies*, 2021; 4, 12(112): 6–17. <https://doi.org/10.15587/1729-4061.2021.238634>
- Kvasnytskyi V., Korzhyk V., Kvasnytskyi V., Mialnitsa H., Dong C., Pryadko T., Matviienko M., Buturlia Y. Designing brazing filler metal for heat-resistant alloys based on Ni3Al intermetallic. *Eastern-European Journal of Enterprise Technologies*. 2020; 6(12): 6–19. <https://doi.org/10.15587/1729-4061.2020.217819>
- Fialko, N.M., Prokopov, V.G., Meranova, N.O.,

- Borisov Yu.S., Korzhik, V.N., Sherenkovskaya, G.P. Temperature conditions of particle-substrate systems in a gas-thermal deposition process. *Fizika i Khimiya Obrabotki Materialov*, 1994; 2: 59–67.
6. Fialko, N.M., Prokopov, V.G., Meranova, N.O., Borisov Yu., Korzhik, V.N., Sherenkovskaya, G.P. Thermal physics of gasothermal coatings formation processes. State of investigations. *Fizika i Khimiya Obrabotki Materialov*, 1993; 4: 83–93.
 7. Krikent I.V., Krivtsun I.V., Demchenko V.F. Modelling of processes of heat-, mass- and electric transfer in column and anode region of arc with refractory cathode. *The Paton Welding Journal*, 2012; 3: 2–6. <http://dspace.nbu.gov.ua/handle/123456789/101111>
 8. Korzhik V.N. Theoretical analysis of the conditions required for rendering metallic alloys amorphous during gas-thermal spraying. III. Transformations in the amorphous layer during the growth process of the coating. *Soviet Powder Metallurgy and Metal Ceramics*, 1992; 31(11): 943–948. <https://doi.org/10.1007/BF00797621>
 9. Prokopov V.G., Fialko N.M., Sherenkovskaya G.P., Murashov A.P., Korzhik V.N. Effect of the coating porosity on the processes of heat transfer under, gas-thermal atomization. *Powder Metallurgy and Metal Ceramics*, 1993; 32: 118–121. <https://doi.org/10.1007/BF00560034>
 10. Lindgren L.-E. Finite element modeling and simulation of welding part 1: increased complexity. *Journal of Thermal Stresses*, 2001; 24(2): 141–192. <https://doi.org/10.1080/01495730150500442>
 11. Salvati E., Everaerts J., Kageyama K., Korsunsky A.M. Transverse fatigue behaviour and residual stress analyses of double sided FSW aluminium alloy joints. *Special Issue: Advances in Fatigue and Fracture - Celebrating the 40th Anniversary of FFEMS*, 2019; 42(9): 1980–1990. <https://doi.org/10.1111/ffe.13068>
 12. Repin S.I., Sauter S.A. Accuracy of Mathematical Models. *Jahresbericht der Deutschen Mathematiker-Vereinigung*, 2020; 122: 269–274. <https://doi.org/10.1365/s13291-020-00222-0>
 13. Buhaienko I., Kyrylenko M., Mylenkyi V. Mathematical modeling of the technological process and synthesis of the amidation control system. *Proceedings of the NTUU “Igor Sikorsky KPI” Series Chemical engineering ecology and resource saving*, 2022; 1(21): 55–61. <https://doi.org/10.20535/2617-9741.1.2022.254159>
 14. Bajuri M. R., Siri Z., Abdullah M. N. S. Mathematical modeling research output impacting new technological development: An axiomatization to build novelty. *Axioms* 2022; 11(6): 264. <https://doi.org/10.3390/axioms11060264>
 15. Anca A., Cardona A., Risso J., Fachinotti V. D. Finite element modeling of welding processes. *Applied Mathematical Modelling*, 2011; 35(2): 688–707. <https://doi.org/10.1016/j.apm.2010.07.026>
 16. Kik T. Numerical analysis of MIG welding of butt joints in aluminium allo. *Institute of Welding Bulletin*, 2014; 3: 37–45.
 17. Livieri P., Tovo R. Optimization of welded joints under fatigue loadings. *Metals*, 2024; 14(6): 613. <https://doi.org/10.3390/met14060613>
 18. Chandramohan D. L., Roy K., Taheri H., Karpenko M., Fang Z., Lim J. B. P. A State of the art review of fillet welded joints. *Materials*, 2022; 24: 8743. <https://doi.org/10.3390/ma15248743>
 19. James M., Hughes D., Hattingh D.G., Mills G., Webster P.J. Residual stress and strain in MIG butt welds in 5083-H321 aluminium: As-welded and fatigue cycled. *International Journal of Fatigue*, 2009; 31(1): 28–40. <https://doi.org/10.1016/j.ijfatigue.2008.04.010>
 20. Ma M., Lai R., Qin J., Wang B., Liu H., Yi D. Effect of weld reinforcement on tensile and fatigue properties of 5083 aluminum metal inert gas (MIG) welded joint: Experiments and numerical simulations. *International Journal of Fatigue*, 2021; 144: 106046. <https://doi.org/10.1016/j.ijfatigue.2020.106046>
 21. Khoshroyan A., Darvazi A. R. Effects of welding parameters and welding sequence on residual stress and distortion in Al6061-T6 aluminum alloy for T-shaped welded joint. *Transactions of Nonferrous Metals Society of China*, 2020; 30(1): 76–89. [https://doi.org/10.1016/S1003-6326\(19\)65181-2](https://doi.org/10.1016/S1003-6326(19)65181-2)
 22. Chaurasia P.K., Pandey C., Giri A., Saini N., Mahapatra M.M. A comparative study of residual stress and mechanical properties for FSW and TIG weld on structural steel. *Arch. Metall. Mater.* 2018; 63(2): 1019–1029. <https://doi.org/10.24425/122437>
 23. Song G., Wang Z., Fan X., Liu L. Research Progress of Aluminum Alloy Welding/Plastic Deformation Composite Forming Technology in Achieving High-Strength Joints. *Materials (Basel)*, 2023; 16(24): 7672. <https://doi.org/10.3390/ma16247672>
 24. Zhang T., Chen J., Gong H., Li H. Study on Residual Stresses of 2219 Aluminum Alloy with TIG Welding and Its Reduction by Shot Peening. *Metals*, 2023; 13(9), 1581. <https://doi.org/10.3390/met13091581>
 25. Wang J., Chen X., Yang L., Zhang G. Effect of preheat & post-weld heat treatment on the microstructure and mechanical properties of 6061-T6 aluminum alloy welded sheets. *Materials Science and Engineering: A*, 2022; 841: 143081. <https://doi.org/10.1016/j.msea.2022.143081>
 26. Macek W., Sampath D., Pejkowski Ł., Żak K. A brief note on monotonic and fatigue fracture events investigation of thin-walled tubular austenitic steel specimens via fracture surface topography analysis (FRASTA). *Engineering Failure Analysis*,

- 2022; 134: 106048. <https://doi.org/10.1016/j.engfailanal.2022.106048>
27. Macek W., Tomczyk A., Branco R., Dobrzyński M., Seweryn A. Fractographical quantitative analysis of EN-AW 2024 aluminum alloy after creep pre-strain and LCF loading. *Engineering Fracture Mechanics*, 2023; 282: 109182. <https://doi.org/10.1016/j.engfracmech.2023.109182>
 28. Nie F., Dong H., Chen S., Li P., Wang L., Zhao Z., Li X., Zhang H. Pulse MIG welded 6061/A356 aluminum alloy dissimilar butt joints. *Journal of Materials Science & Technology*, 2018; 34(3): 551–560. <https://doi.org/10.1016/j.jmst.2016.11.004>
 29. Liu A., Tang X., Lu F. Study on welding process and prosperities of AA5754 Al-alloy welded by double pulsed gas metal arc welding. *Materials & Design*, 2013; 50: 149–155. <https://doi.org/10.1016/j.matdes.2013.02.087>
 30. Cao S.-F., Chen T.-P., Yi J., Guo P., Li L. Simulation of temperature, stress and deformation during double pulsed MIG welding of aluminum alloy. *The Chinese Journal of Nonferrous Metals*, 2014; 24(7): 1685–1692. <https://doi.org/10.19476/j.ysxb.1004.0609.2014.07.001>
 31. Xu S., Chen J., Shen W., Hou R., Wu Y. Fatigue strength evaluation of 5059 aluminum alloy welded joints Considering welding deformation and residual stress. *International Journal of Fatigue*, 2022; 162: 106988. <https://doi.org/10.1016/j.ijfatigue.2022.106988>
 32. Labur T.M. Welded structures from aluminium alloys. *he Paton Welding Journal*, 2020; 3: 25–33. <https://doi.org/10.37434/tpwj2020.03.04>
 33. Chen B.-Q., Liu K., Xu S. Recent advances in aluminum welding for marine structures. *Journal of Marine Science and Engineering*, 2024; 12(9): 1539. <https://doi.org/10.3390/jmse12091539>
 34. Kuchuk-Yatsenko S.I., Hushchyn K.V., Ziakhor I.V., Samotryasov S.M., Zavertannyi M.S. and Levchuk A.M. Structure and mechanical properties of 2219-T87 aluminium alloy joints produced by flash butt welding *The Paton Welding Journal*, 2021; 8: 27–32. <https://doi.org/10.37434/tpwj2021.08.06>
 35. Sun Y. The use of aluminum alloys in structures: Review and outlook. *Structures*, 2023; 57: 105290. <https://doi.org/10.1016/j.istruc.2023.105290>
 36. Vander Voort G.F. *Metallography: Principles and Practice – ASM International*, Materials Park, OH, 1999; 752.
 37. Gorowitz B., Saia R.J., Balch E.W. Chapter 4 – Methods of Metal Patterning and Etching, Editor(s): Einspruch N. G., Cohen S. S., Gildenblat G. Sh., *VLSI Electronics Microstructure Science*, Elsevier, 1987; 15 : 159–219. <https://doi.org/10.1016/B978-0-12-234115-1.50008-8>
 38. Gu Y., Zhang W., Xu Y., Shi Y., Volodymyr K. Stress-assisted corrosion behaviour of Hastelloy N in FLiNaK molten salt environment. *npj Materials Degradation*, 2022; 6(1): 90. <http://dx.doi.org/10.1038/s41529-022-00300-x>
 39. Youwei X., Xuqian H., Yu S., Wenzhu Z., Yufen G., Changgen F., Volodymyr K. Correlation between the microstructure and corrosion behaviour of copper/316 L stainless-steel dissimilar-metal welded joints. *Corrosion Sci.*, 2021; 191: 109729. <https://doi.org/10.1016/j.corsci.2021.109729>
 40. Skorokhod A.Z., Sviridova I.S., Korzhik V.N Structural and mechanical properties of polyethylene terephthalate coatings as affected by mechanical pretreatment of powder in the course of preparation. *Mekhanika Kompozitnykh Materialov*, 1994; 30(4): 455–463.
 41. Fialko N., Dinzhos R., Sherenkovskii N. Meranova S. Aloshko D. Izvorska Korzhyk V., Lazarenko M., Mankus I., Nedbaievskia L. Establishment of regularities of influence on the specific heat capacity and thermal diffusivity of polymer nanocomposites of a complex of defining parameters. *Eastern-European Journal of Enterprise Technologies*, 2021; 6(12(114)): 6–12. <http://dx.doi.org/10.15587/1729-4061.2021.245274>
 42. Fialko N., Dinzhos R., Sherenkovskii J., Meranova N., Korzhyk V., Lazarenko M., Koseva N. Establishing Patterns In The Effect Of Temperature Regime When Manufacturing Nanocomposites On Their Heat-Conducting Properties. *Eastern-European Journal of Enterprise Technologies*, 2021; 4(5(112)): 21–26. <http://dx.doi.org/10.15587/1729-4061.2021.236915>
 43. Colegrove P., Ikeagu C., Thistlethwaite A., Williams S. Welding process impact on residual stress and distortion. *Science and Technology of Welding & Joining*, 2009; 14(8): 717–725. <https://doi.org/10.1179/136217109X406938>
 44. Colegrove P., Ikeagu C., Thistlethwaite A., Williams S., Nagy T., Suder W., Steuwer A., Pirling T. Welding process impact on residual stress and distortion. *Science and Technology of Welding and Joining*, 2013; 14, 2009(8): 717–725. <https://doi.org/10.1179/136217109X406938>
 45. Sun J., Nitschke-Pagel T., Dilger K. Generation and distribution mechanism of welding-induced residual stresses. *Journal of Materials Research and Technology*, 2023; 27: 3936–3954. <https://doi.org/10.1016/j.jmrt.2023.10.252>
 46. Zhu S., Wang Q. W., Wang X. M., Han G. F. Analysis on Thermal Efficiency and Softening Behavior of MIG Welding with Longitudinal Magnetic Field. *Advanced Materials Research*, 2010; 148–149: 326–331. <https://doi.org/10.4028/www.scientific.net/AMR.148-149.326>
 47. Tsaryk B.R., Muzhichenko O.F., Makhnenko O.V. Mathematical model of determination of residual

- stresses and strains in friction stir welding of aluminium alloy. *The Paton Welding Journal*, 2022; 9: 33–40. <https://doi.org/10.37434/tpwj2022.09.06>
48. Tsaryk B.R., Makhnenko O.V. Mathematical modelling of distortions at welding of large vessels of aluminium alloy. *The Paton Welding Journal*, 2024; 8: 18–25. <https://doi.org/10.37434/tpwj2024.08.03>
49. Makhnenko O.V., Muzhichenko A.F. Mathematical modelling of thermal straightening of cylindrical shells and shafts with distortions along their longitudinal axis. *The Paton Welding Journal*, 2007; 9: 17–22.
50. Zienkiewicz O.C., Taylor R.L., Fox D.D. *The Finite Element Method for Solid and Structural Mechanics*, 7th Edition, Elsevier, 2014; 657.
51. Goldak J.A., Akhlaghi M. *Computational welding mechanics*. – O.: USA, Springer, 2005; 325. <https://doi.org/10.1007/b101137>
52. Zhernosekov A., Fedorchuk V., Novomlynets O. Regulation of current pulse parameters during MIG welding of aluminum alloys. *Technical Sciences and Technologies*, 2022; 2(28): 31–37. [https://doi.org/10.25140/2411-5363-2022-2\(28\)-31-37](https://doi.org/10.25140/2411-5363-2022-2(28)-31-37)
53. Wang Y.-Z., Li G.-Q., Wang Y.-B., Lyu Y.-F. Simplified method to identify full von Mises stress-strain curve of structural metals. *Journal of Constructional Steel Research*, 2021; 181: 106624. <https://doi.org/10.1016/j.jcsr.2021.106624>